THE BREMSSTRAHLUNG WEIGHTED CROSS SECTION AND TWO-BODY CORRELATIONS IN NUCLEI*

W.T. WENG and T.T.S. KUO
Department of Physics, State University of New York, Stony Brook, New York 11794, USA

and

K.F. RATCLIFF
Department of Physics, State University of New York, Albany, New York 1222, USA

Received 3 August 1974

The effect of two-body correlations on the calculation of the bremsstrahlung weighted cross section σ_{-1} is investigated for ^{4}He, ^{16}O and ^{40}Ca by making partial sums of the linked cluster expansion. It is found that σ_{-1} is sensitive to long-range correlations but is quite insensitive to the inclusion of short-range correlations.

A recent investigation by Weng, Kuo and Brown [1] showed the electric dipole sum rule to be strongly sensitive to the short-range two-body correlations in nuclei. The inclusion of such correlations was found to nearly double the electric dipole enhancement factor. Similar assessment of the role played by such correlations has been reported for Coulomb matrix elements [2] and muon capture matrix elements [3].

This program is continued in the present work by investigating whether the bremsstrahlung weighted cross section shows a similar sensitivity to short-range correlations. A second objective is to clarify the theoretical framework within which the search for the effects of short-range correlations is being conducted.

The bremsstrahlung weighted sum rule [4] is given by

$$\sigma_{-1} = \int \frac{\sigma}{E}\, \mathrm{d}E = \frac{4\pi^2}{3\hbar c} \sum_n \langle 0|\boldsymbol{D}|n\rangle\langle n|\boldsymbol{D}|0\rangle \qquad (1)$$

where the dipole operator $\boldsymbol{D}$ is given by

$$\boldsymbol{D} = -e \sum_{i=1}^{A} t_{3i} \boldsymbol{r}_i$$

and where $\boldsymbol{r}_i$ is the position of the ith nucleon relative to the nuclear center of mass ($\Sigma_{i=1}^{A} \boldsymbol{r}_i = 0$) and t_{3i} is the third component of the isospin having eigenvalue $-1/2$ for protons and $+1/2$ for neutrons. The sum runs over all states $|n\rangle$ coupled to the true ground state $|0\rangle$ by $\boldsymbol{D}$.

In the present work we restrict our attention to three doubly closed shell nuclei with $N = Z$(^{4}He, ^{16}O, ^{40}Ca). When closure is then applied in (1) only the completely scalar part of $\boldsymbol{D}\times\boldsymbol{D}$ survives and (1) reduces to

$$\sigma_{-1} = \frac{4\pi^2 e^2}{3\hbar c} \langle 0|\theta|0\rangle \qquad (2)$$

where

$$\theta = \tfrac{1}{3} \sum_i \sum_j (\boldsymbol{r}_i\cdot\boldsymbol{r}_j)(\boldsymbol{t}_i\cdot\boldsymbol{t}_j)$$

$$= \tfrac{1}{4} \sum_i r_i^2 + \tfrac{2}{3} \sum_{i<j} (\boldsymbol{t}_i\cdot\boldsymbol{t}_j)(\boldsymbol{r}_i\cdot\boldsymbol{r}_j) \qquad (3)$$

It is essential to reexpress θ in a way to accommodate consideration of the pairwise correlation of nucleons. We thus transform to two-nucleon center-of-mass variables ($\boldsymbol{r}_{ij} = \boldsymbol{r}_i - \boldsymbol{r}_j$ and $\boldsymbol{R}_{ij} = \frac{1}{2}(\boldsymbol{r}_i + \boldsymbol{r}_j)$) and express the one-body operator in (3) as a two-body operator

$$\sum_{i<j} (\boldsymbol{t}_i\cdot\boldsymbol{t}_j)(\boldsymbol{r}_i\cdot\boldsymbol{r}_j) = \sum_{i<j} (\boldsymbol{t}_i\cdot\boldsymbol{t}_j)(R_{ij}^2 - \tfrac{1}{4} r_{ij}^2) \qquad (4)$$

$$\sum_i r_i^2 = \frac{2}{A-1} \sum_{i<j} (R_{ij}^2 + \tfrac{1}{4} r_{ij}^2). \qquad (5)$$

The fact that the two-body operator in (5) is really a

* Work supported by the United States Atomic Energy Commission under Contract AT(11-1)-3001.

one-body operator in disguise is evident by its singular nature for $A = 1$. The final expression for θ as a two-body operator is

$$\theta = \sum_{i<j} \left\{ \tfrac{1}{2} \frac{1}{A-1} (R_{ij}^2 + \tfrac{1}{4} r_{ij}^2) + \tfrac{2}{3} (t_i \cdot t_j)(R_{ij}^2 - \tfrac{1}{4} r_{ij}^2) \right\}. \quad (6)$$

The ground state expectation value of a scalar operator θ for a doubly closed shell nucleus is given by the sum of all linked Goldstone diagrams in which the θ-vertex appears exactly one time [5]. It should be emphasized that this statement of the diagrammatic expansion for $\langle\theta\rangle$ is properly normalized, i.e.

$$\langle\theta\rangle = \frac{\langle\bar{\Psi}|\theta|\bar{\Psi}\rangle}{\langle\bar{\Psi}|\bar{\Psi}\rangle} \quad (7)$$

where $|\bar{\Psi}\rangle$ is the true many-body ground state. The connection of (7) with diagrams is provided by expressing $|\bar{\Psi}\rangle$ as the adiabatic limit of the time evolution operator $U(0,-\infty)$ operating on the unperturbed many-body ground state $|\Phi\rangle$ of H_0 [6, 7]

$$H_0|\Phi\rangle = E_0|\Phi\rangle, \qquad (H_0 + H_1)|\bar{\Psi}\rangle = E|\bar{\Psi}\rangle,$$

$$|\bar{\Psi}\rangle = \frac{U(0,-\infty)|\Phi\rangle}{\langle\Phi|U(0,-\infty)|\Phi\rangle}, \qquad \langle\bar{\Psi}| = \frac{\langle\Phi|U(\infty,0)}{\langle\Phi|U(\infty,0)|\Phi\rangle}, \quad (8)$$

$$\langle\Phi|\bar{\Psi}\rangle = \langle\bar{\Psi}|\Phi\rangle = 1.$$

Proof of the linked diagram series for $\langle\theta\rangle$ can be obtained by directly making a diagrammatic expansion of the ground state as it appears in (7). However, the same result follows quickly by appeal to the "linked cluster theorem" for the ground state correlation energy ΔE. One then considers the correlation energies for a pair of related hamiltonians

$$\Delta E = E - E_0 = \frac{\langle\Phi|H - H_0|\bar{\Psi}\rangle}{\langle\Phi|\bar{\Psi}\rangle} \quad (9)$$

$$\Delta E' = E' - E_0 = \frac{\langle\Phi|H' - H_0|\bar{\Psi}'\rangle}{\langle\Phi|\bar{\Psi}'\rangle} \quad (10)$$

where E' and $|\bar{\Psi}'\rangle$ are the true ground state energy and eigenfunction for $H' = H + \lambda\theta$ [7]. Both (9) and (10) are given by the sum of all linked Goldstone diagrams. However the expansion for (10) contains, in addition to all the diagrams for (9), diagrams with one or more θ-vertices. However in the limit

$$\langle\theta\rangle = \lim_{\lambda\to 0} \left(\frac{\Delta E' - \Delta E}{\lambda} \right) \quad (11)$$

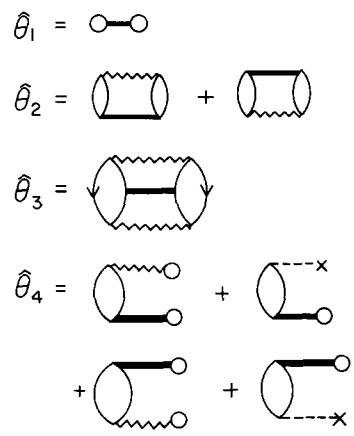

Fig. 1. Diagrams evaluated in calculating $\langle\theta\rangle$. The two-body vertex represented by the wavy line is the reaction matrix. The two-body vertex represented by the solid bar is the renormalized operator $\hat{\theta}$. The particle lines in these diagrams are confined to the first major shell lying above the p-h vacuum. The one-body vertex (---X) represents a $-U$ insertion, where U is the single particle potential included in H_0.

it is clear that only the diagrams which are linear in λ will survive. These of course are the diagrams with exactly one θ-vertex.

The actual set of "two hole-line diagrams" that were summed to evaluate $\langle\theta\rangle$ are shown in fig. 1. These have been divided into four classes denoted by $\hat{\theta}_i (i = 1,4)$ and

$$\langle\theta\rangle \approx \hat{\theta}_1 + \hat{\theta}_2 + \hat{\theta}_3 + \hat{\theta}_4. \quad (12)$$

Clearly $\hat{\theta}_4 = 0$ in a Brueckner-Hartree-Fock representation. The renormalized operator vertex $\hat{\theta}$ displayed in fig. 1 arises by summing a subset of linked Goldstone diagrams in which the vertex θ is evaluated between uncorrelated two particle states. These two particle states include both low-lying states that reflect the long-range two-body correlations and high-lying states involved in G-matrix interactions and which reflect the short-range two-body correlations induced by the nucleon-nucleon interaction. The subset of linked diagrams which is to be added is chosen so that the resulting sum is given by a matrix element of θ between correlated low-lying two particle states. In this way the effect of the short-range part of the two-body correlation on the expectation value of θ is being treated in precise analogy to the way G replaces V as the first step in achieving an effective interaction. An example

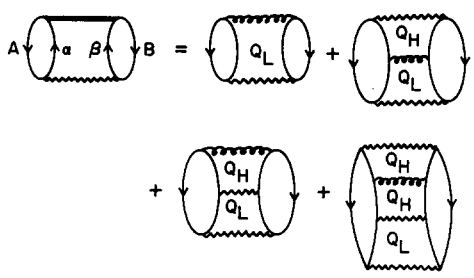

Fig. 2. Diagrams involving the vertex θ, denoted by "inductance" line, which sum to yield the renormalized vertex θ, denoted by solid bar. The two-body projection operators Q_L and Q_H which determine the intermediate states are defined in fig. 3.

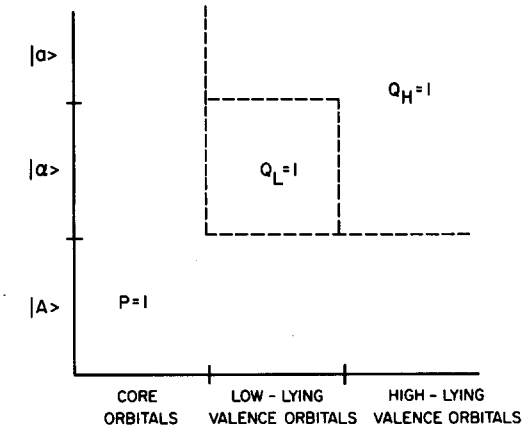

Fig. 3. The two-body projection operators ($P+Q_L+Q_H=1$) defined by the single particle representation of H_0.

of such a subset of linked diagrams is shown in fig. 2. Each of the other diagrams in fig. 1 may likewise be expressed as a sum of four linked Goldstone diagrams involving the unrenormalized θ-vertex. The value of the renormalized $\hat{\theta}$-vertex in fig. 2 is given by

$$\langle\phi_{AB}|\hat{\theta}|\phi_{\alpha\beta}\rangle = \langle\phi_{AB}|\Omega^{+}\theta\Omega|\phi_{\alpha\beta}\rangle$$

$$= \langle\psi_{AB}|\theta|\psi_{\alpha\beta}\rangle = \langle(\phi-\chi)_{AB}|\theta|(\phi-\chi)_{\alpha\beta}\rangle \qquad (13)$$

where ϕ and ψ are respectively and uncorrelated and correlated two particle wave functions, χ is the defect wave function, and Ω is the wave operator defined by

$$\Omega\phi=\psi=\phi-\chi, \quad \Omega=1+G\frac{Q_H}{e}, \quad G=V+V\frac{Q_H}{e}G. \qquad (14)$$

The diagrammatic equality as expressed in fig. 2 has clearly employed a propagator with $e=\omega-H_0$. However it is also clear that by adding diagrams with all possible $-U$ insertions we can obtain the more fundamental renormalized $\hat{\theta}$ defined by the propagator $e=\omega-Q_H T Q_H$ in (14).

The two-particle projection operators Q_H and Q_L are defined in fig. 3. The core orbitals are denoted by capital letters and define the p-h vacuum of H_0. The low-lying valence orbitals, denoted by Greek letters, are here restricted to one major shell outside the p-h vacuum. The high-lying valence orbitals are denoted by lower case letters and lie more than one major shell beyond the p-h vacuum. The high lying, intermediate, two particle states define Q_H which in turn serves as the Pauli operator in the definition of G in (14). The two particle intermediate states in fig. 1 are restricted to the finite set defined by Q_L. This restriction then removes any question of the double counting of histories due to the role played by G in the definition of $\hat{\theta}$.

The results of the present calculation are listed in table 1. Here we show the contribution to σ_{-1} from each class of diagrams defined in fig. 1, i.e. $\sigma_{-1}(\mathrm{i}) = (4\pi e^2/3\hbar c)\hat{\theta}_i$. These calculations were performed using the oscillator hamiltonian for H_0. The designation *no correlation* indicates that the matrix elements of θ in (13) were calculated with $\chi=0$. In fig. 2 this would correspond to keeping just the first diagram. The results *with correlation* employed the reference spectrum approximation for χ in (13), i.e.

$$|\chi_R\rangle = -\frac{1}{k^2+\gamma^2}G|\phi\rangle$$

with a gap parameter $\gamma^2=4$. It should be noted that χ is a function only of the two particle separation r_{ij}. Thus the inclusion of χ in the calculation of σ_{-1} does not affect those parts of θ in (6) which depend only on the position of the two particle center-of-mass R_{ij}. The experimental values for σ_{-1} are taken from the recent compilation by Fuller et al. (8).

It is observed that the calculated results for σ_{-1} agree well with the empirical data for all three nuclei. Of greater interest is the fact that the use of the correlated wave function is seen to have very little effect on the matrix elements of θ. It is thus concluded that the bremsstrahlung weighted sum rule is quite insensitive to the short-range two-body correlations in nuclei.

Table 1
Contributions to the bremsstrahlung-weighted cross section. The separate contributions are in units of mb and correspond to the classes of diagrams in fig. 1.

		$\sigma_{-1}(1)$	$\sigma_{-1}(2)$	$\sigma_{-1}(3)$	$\sigma_{-1}(4)$	Total	Experiment
^{4}He	No correlation	3.15	−0.70	0.06	–	2.51	2.2
	With correlation	3.35	−0.69	0.06	–	2.72	
^{16}O	No correlation	17.08	−3.19	−0.73	−0.13	13.03	14
	With correlation	17.80	−3.15	−0.72	−0.12	13.80	
^{40}Ca	No correlation	56.94	−9.57	−2.11	−0.96	44.31	42
	With correlation	58.61	−9.53	−2.10	−0.92	46.06	

Finally we observe rather rapid convergence in the inclusion of diagrams which are higher order in the number of G-vertices coupled to θ through the two-body projector Q_L; namely $\sigma_{-1}(2)$ is much smaller than $\sigma_{-1}(1)$ and $\sigma_{-1}(3)$ is in turn much smaller than $\sigma_{-1}(2)$.

In table 1, the values given for $\sigma_{-1}(1)$ with *no* correlation are usually referred to as the "shell-model value" for the bremsstrahlung weighted cross section. This shell model value is consistently larger than the experimental value. The values given for $\sigma_{-1}(2)$, $\sigma_{-1}(3)$ and $\sigma_{-1}(4)$ with *no* correlation represent corrections from low-lying core excitations and are thus usually referred to as reflecting long-range two-body correlations. These alone are seen to yield good agreement between σ_{-1} ane experiment and is consistent with the observations of Lane and Mekjian [9]. The additional corrections seen by comparing σ_{-1}(i) *with* and *without* correlations show the very small influence of the short-range two-body correlations.

It is easily understood why the present result is so different from that found earlier for the electric-dipole sum rule [1]. The pertinent amplitudes which enter σ_{-1} involve matrix elements of r^2 while those in the E1 sum rule involve matrix elements of r^2V. Matrix elements of r^2 necessarily emphasize large separations of the nucleon pair where rapid healing of the pair wavefunction guarantees relative insensitivity to the inclusion of χ. By contrast, the weighting provided by the potential in matrix elements of r^2V emphasizes an intermediate range of 1 to 2 fm separation where χ is appreciable. In addition, the presence of the tensor force in r^2V permits a coupling of channels that was found to be of great importance for the E1 sum rule. No analogous process occurs here for the purely scalar operator r^2. Finally the calculation of the E1 enhancement factor involves the true ground state expectation value of $[[V,D],D]$. The contribution in D due to the two-body center-of-mass R_{ij} does not survive the double commutator whereas the present calculation involves R_{ij}^2 with equal importance to that of r_{ij}^2. As an example, the largest changes in $\langle r^2\rangle$ are of course revealed in the S-channels. The radial integral entering the uncorrelated expectation value for $\langle nl|r^2|nl\rangle$ is 8.89 fm^2 when $n = l = 0$. The $^1S_0$ correlated wave function increases this value to 9.20 fm^2 whereas a value of 9.93 fm^2 is found using the $^3S_1$ correlated wave function. The $n = 0$, $l = 2$ radial integral is increased from 20.75 fm^2 to only 20.93 fm^2.

Recently the authors [10] have determined a practical method for ensuring accurate calculation of the defect wave function χ. A careful analysis of ^{4}He revealed characteristic differences between the true defect wave function and its reference spectrum approximation over an intermediate range of separations However longer range separations are emphasized in the evaluation of $\langle r^2\rangle$. For such separations the correlated wave function has healed and therefore χ is small in value. It thus appears quite unlikely that the present results for σ_{-1} would be materially affected by the more accurate treatment of χ.

This contrast between the dipole cross section, $\sigma_0 = \int \sigma_\gamma(E)\, dE$, and the bremsstrahlung weighted cross section, $\sigma_{-1} = \int \sigma_\gamma(E) E^{-1}\, dE$, may be inferred from the form of these cross sections. The inclusion of the E^{-1} weighting factor in the definition of σ_{-1} would be expected to reduce the relative importance of high-lying states in σ_{-1} compared to that in σ_0. Since these are precisely the states which are used to define G and hence to generate χ, it suggests the relative unimportance of short-range correlations in σ_{-1}. The present calculations provide strong quantitative support for that intuition.

References

[1] W.T. Weng, T.T.S. Kuo and G.E. Brown, Phys. Lett. 46B (1973) 329.

[2] R.K. Anderson, M.R. Wilson and P. Goldhammer, Phys. Rev. C6 (1972) 136;
R.K. Anderson and P. Goldhammer, Phys. Rev. Lett. 26 (1971) 978;
R.J. McCarthy and G.E. Walker, Phys. Rev. C9 (1974) 809;
P. Goldhammer, Phys. Rev. C9 (1974) 813.

[3] R.J. McCarthy and G.E. Walker, preprint.

[4] E. Hayward, B.F. Gibson and J.S. O'Connell, Phys. Rev. C5 (1972) 846.

[5] D. Thouless, The quantum mechanics of many-body systems (Academic Press, New York, 1961).

[6] M. Gell-Mann and F. Low, Phys. Rev. 84 (1951) 350.

[7] T.T.S. Kuo, S.Y. Lee and K.F. Ratcliff, Nucl. Phys. A176 (1971) 65.

[8] E.G. Fuller, H.M. Gerstenberg, H. Vander Molen and T.G. Dunn, Photonuclear Reaction Data, 1973, NBS Special Publication #380 (U.S. Dept. of Commerce, Washington).

[9] A.M. Lane and A.Z. Mekjian, Phys. Lett. 43B (1973) 105.

[10] W.T. Weng, T.T.S. Kuo and K.F. Ratcliff, to be published.